Assembling a true 'Olympic Gel' from >16,000 combinatorial DNA rings

Sarah Speed[1,2,#], Azra Atabay[1,2,#], Yu-Hsuan Peng[1,2], Krishna Gupta[1,2], Toni Müller[3,4], Carolin Fischer[5], Jens-Uwe Sommer[3,4,6], Michael Lang[3,*], Elisha Krieg[1,2,*]

[1]Institute for Biofunctional Polymer Materials, Leibniz Institute of Polymer Research Dresden, Germany; [2]Faculty of Chemistry and Food Chemistry, Technische Universität Dresden, Germany; [3]Institute Theory of Polymers, Leibniz Institute of Polymer Research Dresden, Germany; [4]Institute for Theoretical Physics, Technische Universität Dresden, Germany; [5]B CUBE - Center for Molecular Bioengineering, Technische Universität Dresden, Germany. [6]Cluster of Excellence Physics of Life, Technische Universität Dresden, Germany

# Authors contributed equally.
* To whom correspondence should be addressed: krieg@ipfdd.de, lang@ipfdd.de

Keywords: DNA nanotechnology, supramolecular chemistry, Olympic gels, programmable materials, soft matter engineering, simulations

Abstract

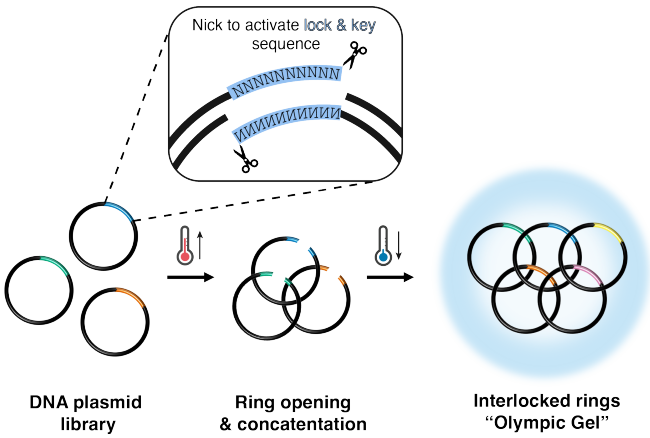

Olympic gels are an elusive form of soft matter, comprising a three-dimensional network of mechanically interlocked cyclic molecules. In the absence of defined network junctions, the high conformational freedom of the molecules was previously theorized to confer unique mechanical properties to Olympic gels, such as non-linear elasticity and unconventional swelling characteristics. However, the synthesis of an Olympic gel exhibiting these intriguing features is challenging, since unintended crosslinking and polymerization processes are often favored over cyclization. Here, we report the successful assembly of a true Olympic gel from a library of DNA rings comprising more than 16,000 distinct molecules. Each of these rings contains a unique sequence domain that can be enzymatically activated to produce reactive termini that favor intramolecular cyclization. We characterized the material's genetic, mechanical, and structural characteristics by next-generation sequencing, oscillatory rheology, large-scale computational simulations, atomic force microscopy, and cryogenic electron microscopy. Our results confirm the formation of a stable Olympic gel, which exhibits unique swelling behavior and an elastic response that is exclusively determined by entanglements, yet persists on long time scales. By combining concepts from polymer physics, synthetic biology, and DNA nanotechnology, this new material class provides a flexible experimental platform for future studies into the effects of network topology on macroscopic material properties and its function as a carrier of genetic information in biological and biomimetic systems. This work moreover demonstrates that exotic material properties can emerge in systems with a high compositional complexity that is more reminiscent of biological than synthetic matter.

Introduction

Gels are versatile soft materials that exhibit unique mechanical and structural properties[1–3]. They consist of molecules that are crosslinked through either chemical bonds or physical (noncovalent) interactions. The resulting three-dimensional molecular network spans the entire volume of the gel, while the interstitial space is filled by a solvent. The interesting properties and functionalities of gels have enabled a wide range of applications, ranging from drug delivery[4], contact lenses[5], and tissue engineering[6] to ultrafiltration membranes[7], autonomously controlled microfluidic channels[8], and light harvesting scaffolds with stimuli-responsive properties[9].

To date, the mechanical properties of gels are explained by relating the modulus (G) to the density of the junctions within the three-dimensional molecular network[10]. If these junctions were removed, the elastic material would turn into a viscous fluid. In 1979, however, De Gennes conjectured[11] that one could make "Olympic gels"—gels entirely devoid of network junctions but instead held together by the concatenation of cyclic molecules (Figure 1a). Interestingly, in the absence of defined network junctions, overlapping rings can be displaced with respect to one another, lowering the entropic cost of macroscopic strain induced by external forces. Due to the topological nature of their crosslinks, Olympic gels are expected to have intriguingly different mechanical properties than classical gels[12], in particular unique deformation[13] and swelling[14] characteristics.

The mechanical interlocking of macrocycles can also serve unique biological functions in nature. The unusual mitochondrial DNA of the microorganism *Kinetoplastea* (known as kinetoplast DNA, or kDNA) consists of several thousand concatenated DNA circles resembling a microscopic two-dimensional version of an Olympic gel[15]. Several members of *Kinetoplastea* are pathogenic parasites that cause dangerous diseases including Chagas disease, African sleeping sickness, and leishmaniasis. The kDNA network plays a critical role in the genetic function, post-transcriptional modifications, and cell division within *Kinetoplastea*, but how its topological structure might influence these biological functions is still under investigation[16,17].

Despite the fascinating mechanical and functional properties of Olympic gels, their synthesis has proven remarkably challenging. Correspondingly, true Olympic gels have to date only been realized in computer simulations[14,18–20]. To form an Olympic gel experimentally, one must achieve efficient cyclization of concentrated linear molecules. The high concentration is necessary as the newly formed macrocycles must overlap in space with other nascent macrocycles to allow the formation of a sample-spanning concatenated network. However, at the required concentrations for proper concatenation, a polymerization process is thermodynamically favored over cyclization for both reversible and irreversible reactions such that the molecules are linked together to form linear chains[21].

In recent decades, several ideas have been proposed to overcome the cyclization-vs-polymerization challenge[22,23]. However, computational simulations indicate that the required experimental conditions are often difficult to achieve in practice[18]. It has been reported that some degree of concatenation can be achieved in mixtures of cyclic polymers[24,25], but to date, there has been no study demonstrating the chemical synthesis of an Olympic gel. Two studies have reported a biologically-inspired approach for the synthesis of an Olympic gel using the help of the enzyme *topoisomerase II* to concatenate plasmid DNA[26,27]. The enzyme transiently breaks and reforms plasmids, thus allowing previously separated DNA strands to pass through each other and thereby to interlock. This approach is elegant; however, there is strong evidence that the enzyme itself forms bridges between the DNA strands and thereby creates

classical network junctions (as suggested by the latest study)[26,28]. The effect of these classical junctions dominates the mechanical characteristics of the material.

In the present study, we report a new approach for generating Olympic gels. This method is based on biotechnologically produced double-stranded DNA rings that are enzymatically processed to reversibly open and close at a predefined position. We have previously shown that the predictable binding selectivity of DNA can be leveraged to favor intermolecular over intramolecular crosslinks in noncovalent molecular networks[29,30]. Here, we demonstrate that a similar approach can be used "in reverse" to favor intramolecular cyclization over intermolecular polymerization. By cloning combinatorial DNA sequence mixtures into *E. coli*, we generated a diverse library of DNA plasmids containing more than 16,000 distinct DNA sequences. These libraries are enzymatically processed, purified, and finally self-assembled to form an Olympic gel, as revealed by oscillatory rheology, electron microscopy, and swelling experiments.

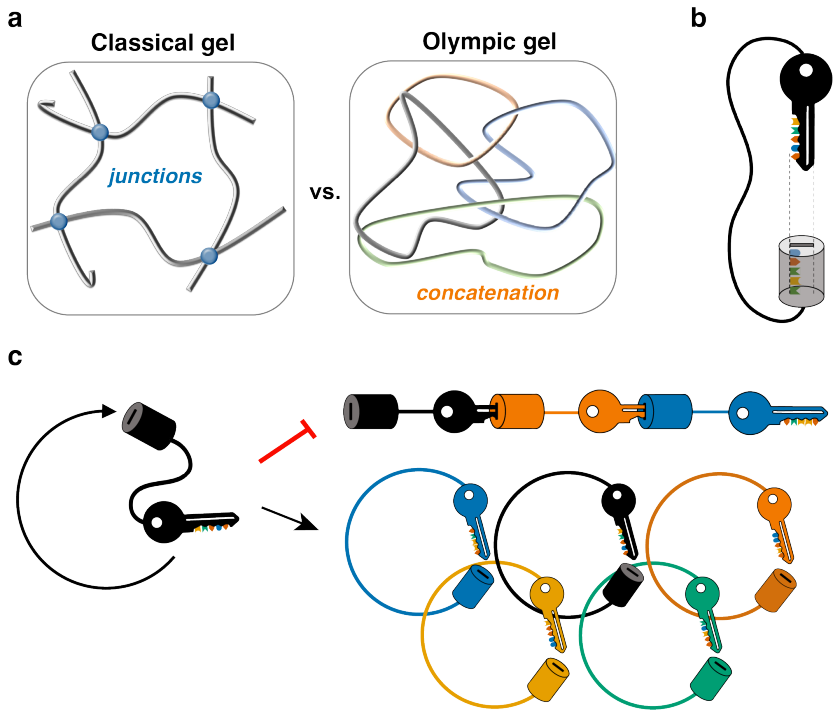

Figure 1. The elusive synthesis of Olympic gels requires molecules that form concatenated rings instead of linear polymers or classical network junctions. a) Comparison between classical gels, which are crosslinked by either covalent or noncovalent junctions, and Olympic gels, which do not have distinct junctions but are held together by mechanically interlocked (concatenated) rings. **b)** Scheme of a hypothetical linear molecule having two reactive termini (a key and a lock) that bind to each other through selective recognition. **c)** The key-in-lock model favors intramolecular binding over intermolecular binding. Given a library of molecules with a sufficient diversity of lock-and-key pairs, the polymerization of linear chains is suppressed, and the formation of an Olympic gel is thermodynamically favored.

Results and Discussion

Concept and computer-assisted material design

To construct an Olympic gel, one needs a molecule that readily becomes mechanically interlocked but does not form classical junctions. We hypothesized that a polymer with two reactive termini would fulfill this requirement if the termini selectively recognize each other

(analogous to a key and lock) but do not bind to other molecules in the vicinity (Figure 1b). To achieve such highly selective cyclization, a diverse mixture of components is needed such that each of the molecules is statistically likely to be surrounded only by molecules carrying different binding sites (Figure 1c). Assuming a large enough diversity of reactive termini, such mixtures are expected to form an Olympic gel at high concentration[22].

However, implementing this concept is not straightforward, as the set of orthogonal binding motifs available in organic or supramolecular chemistry is limited[31,32]. An exception is DNA, whose highly selective Watson-Crick-Franklin base pairing can be used to construct large libraries with orthogonal binding interactions[30,33]. We sought to insert such binding motifs into plasmids, naturally ring-shaped DNA molecules that are expressed in bacteria. To this end, we designed a DNA oligonucleotide termed *DLK* (for "diversified lock & key") for cloning into a plasmid backbone (Figure 2a). The *DLK* insert maximizes sequence complexity in the final plasmid library through the inclusion of a combinatorial *lock & key domain* consisting of 16 mixed nucleotides (N), where each N can be either of the four canonical bases A, T, C, or G with ~25% probability. This approach creates a mixture of 4^{16} (~4 billion) unique lock & key domains. Thus, after the initial assembly, each plasmid contains a distinct lock & key domain that will hybridize with its complement on the same plasmid backbone. The lock & key domain is flanked by two *nicking sites*, specific recognition sequences for the *Nt.BbvCI* nicking endonuclease. Enzymatic nicking on opposite sides of the lock & key domain creates a 20-nucleotide (nt)-long sticky end that can be reversibly opened and closed via thermal or chemical denaturation (Figure 2a). We also included two diversified *strand exchange protector* domains, each consisting of 9 N nucleotides. These domains flank the sticky ends and prevent spurious strand exchange that could otherwise take place at elevated temperature due to strand fraying.

Using nearest-neighbor thermodynamic calculations[34], the 20 nt sticky ends were predicted to bind to each other with a minimum free energy (MFE) of -114 kJ mol^{-1} (46 k_BT), which is approximately one-third of the dissociation energy of a typical covalent bond (see Methods Section). The melting temperature was predicted to be between 50-60°C. We therefore expected that at room temperature most plasmid rings are firmly closed, but at low ionic strength or when annealed near the melting temperature, they would transiently open and allow for subsequent concatenation. To further guide our experimental design, we used bond-fluctuation model (BFM) computer simulation data[35] to predict the critical gelation concentration (c_{gel}) and the average number of expected concatenations per ring (f_n) at different concentrations (Supplementary Section S2, Figure S5). c_{gel} was predicted as 0.11 wt%. This point corresponds to a universal overlap number (P) of P = 0.36, above which a cyclic polymer can form an Olympic gel (see Section S2 for details). For ideal plasmid solutions of constant molar mass, such as for our series of gels, f_n can be estimated as $f_n \approx c/c_{gel}$ [18]. Based on these calculations, we prepared plasmid solutions with weight fractions ranging from approximately one order of magnitude above to one order of magnitude below the predicted value for c_{gel} (0.01 - 0.8 wt%).

Biotechnological production of the Olympic gel

We applied classical cloning techniques for the production of the diverse plasmid library (Figure 2b). We first integrated the *DLK* insert into a *PVS10* plasmid backbone[36] using high-fidelity Gibson assembly[37]. The Gibson product was transformed in five separate batches of *E. coli* cells. These were combined for culture growth on a large scale (2.4-liter volume), and the product was purified to yield ~4 mg of the plasmid library (*PVS10-DLK*). We then digested

the *PVS10-DLK* library with *Nt.BbvCI* nicking endonuclease to activate the *DLK* insert. This product is hereafter referred to as the "nicked" plasmid library. To serve as a reference, we reserved an equivalent sample of the *PVS10-DLK* library that was not subjected to nicking (referred to as the "non-nicked" plasmid library).

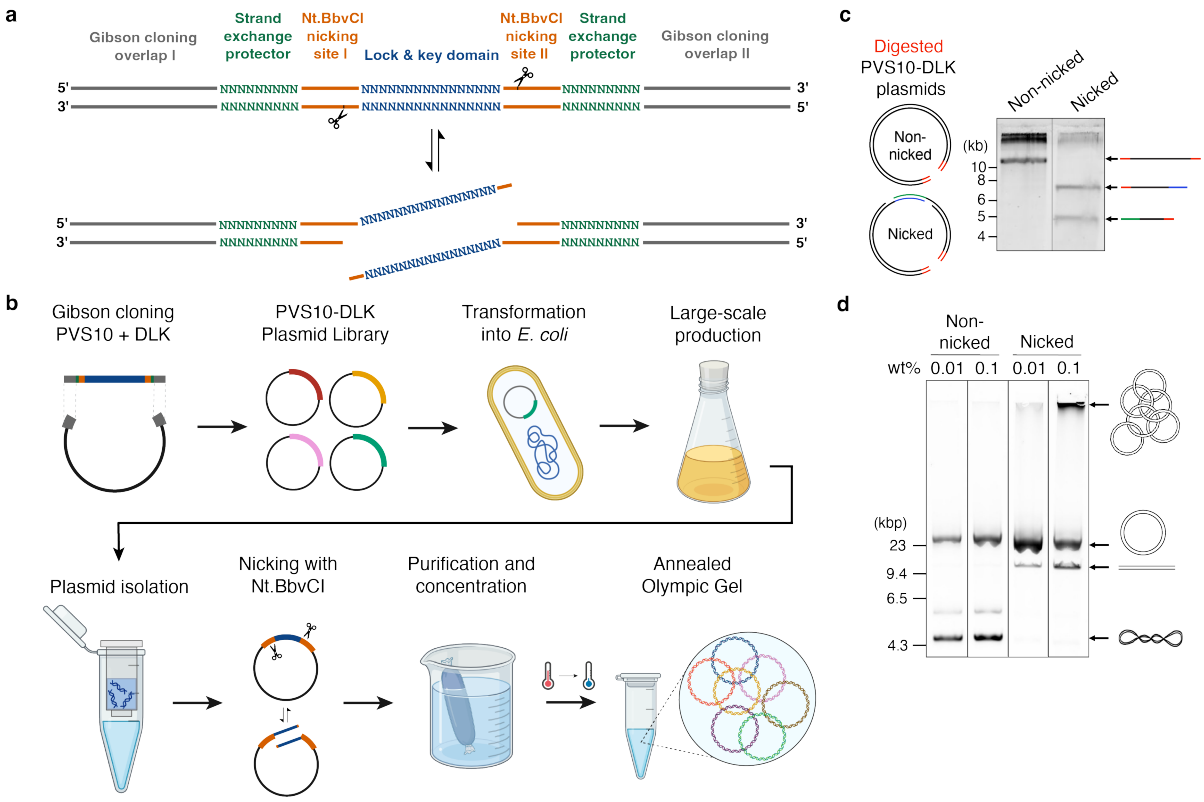

Figure 2. The Olympic gel components are expressed in *E. Coli* and enzymatically processed. a) Design of the *DLK* insert for implementation of the key-in-lock model with DNA plasmid rings. **b)** Schematic depicting the cloning and molecular biology techniques used in the creation of the Olympic gel. **c)** Alkaline denaturing AGE of non-nicked and nicked *PVS10-DLK* libraries demonstrating high nicking efficiency. **d)** Native AGE of non-nicked and nicked *PVS10-DLK* libraries at different concentrations. The band corresponding to mechanically interlocked rings is only observed when the plasmid library is nicked and incubated at a sufficiently high concentration for concatenation to take place.

We tested nicking efficiency through an analytical *HindIII* restriction enzyme digestion targeting the *PVS10* backbone at a site approximately mid-distal from the *DLK* insertion site, followed by denaturing agarose gel electrophoresis (AGE) analysis (Figure 2c). We anticipated that successful nicking would result in two bands, indicative of the linearization of the PVS10 backbone via a double-strand break by *HindIII*, followed by dissociation of the nicked lock & key domain in DLK, while non-nicked plasmids would only become linearized. The complete dissociation of nicked *PVS10-DLK* into two bands, in comparison to the single band of the non-nicked sample, indicated the successful and near-quantitative nicking of the plasmid library.

The *PVS10-DLK* library was subsequently purified via dialysis and concentrated to 0.125, 0.25, 0.5, or 0.8 wt%. The sodium chloride concentration in each sample was adjusted to 50 mM. We avoided higher salt concentrations and made sure to exclude divalent cations, as these promote nonspecific binding between DNA strands[38]. In order to form the final Olympic gel under consistent conditions, we heated the plasmid solutions to a temperature slightly above the predicted melting temperature of the lock & key domain to open the

plasmids and allow the rings to pass through one another, followed by incubation at room temperature to anneal the plasmids into a topological network.

To verify concatenation of the plasmid rings following our annealing protocol, we analyzed both non-nicked and nicked *PVS10-DLK* libraries at different concentrations by native AGE (Figure 2d, Figure S6, and Supplementary section S3). The non-nicked samples contained both supercoiled and relaxed circular forms of the plasmid at approximately equal concentrations. We attribute the presence of the relaxed circular form to mechanical shear during pipetting and sample handling that can introduce random backbone breaks leading to relaxation of some of the supercoiled rings[39]. As expected, the enzymatically nicked samples were virtually free of supercoiled DNA. A minor band corresponding to the linear plasmid form appeared in the nicked sample, which is presumably formed when some of the lock & key domains dissociate during pipetting and sample handling. Importantly, in the nicked sample, a major fraction of DNA is trapped near the well. The intensity of this band in relation to the free circular plasmid band increases with increasing concentration, which is indicative of concatenation of the plasmid rings leading to the formation of larger clusters of rings in solution (Figure 2d). This experiment further demonstrates that ring concatenation requires the fulfillment of two criteria: firstly, the ability of the plasmid rings to reversibly open and close, and secondly, a sufficiently high concentration to allow overlap and concatenation of the rings in solution.

Sequencing reveals highly diversified lock & key domains with orthogonal binding

Achieving a high number of unique sequences within the *DLK* insert of the final plasmid library is key for generating an Olympic gel[18]. We speculated that large-scale expression in *E. coli* could, in principle, lead to distortions in the prevalence of distinct sequences, as some sequences might be preferentially expressed. In order to verify that the plasmid library sequences were still widely distributed after expression, we characterized the *DLK* insert in both the original Gibson product before transformation and the final purified *PVS10-DLK* library by next-generation sequencing on the Illumina MiSeq platform (Figure 3, Supplementary Data 1).

We obtained and analyzed more than 100,000 sequences of properly merged paired end reads for both the Gibson product and final library. Using a custom Python script (Supplementary Code 1), we identified instances of *Nt.BbvCI* nicking sites in order to extract sequences of interest. We found that ~98.5% of the analyzed sequences contained proper nicking sites, both in the initial Gibson product as well as the final library (Figure 3b), demonstrating that *DLK* insertion into the plasmid was highly efficient and that most of the circular DNA product can be activated by the *Nt.BbvCI* nicking enzyme. Importantly, the lock & key domain as well as the two strand exchange protector domains exhibited high sequence diversity in the final library (Figure 3a). A slight bias was found in favor of adenine and thymine (58%) over cytosine and guanine (42%). This bias existed already in the initial Gibson product (Figure S10), likely reflecting a bias in the phosphoramidite-based synthesis of the commercial oligonucleotide[40]. The base frequencies in all variable positions were nearly identical in the Gibson product and the final library indicating that the expression in *E. Coli* did not introduce additional biases for specific bases (Figure 3a, Figure S10).

We then computed the total number and prevalence of unique sequence variants within the *DLK* domain (Figure 3b, c). Within the pool of 140,541 identified sequences in the Gibson product, 125,815 sequences (89.5%) were unique. The single most prevalent sequence in the Gibson product library had a frequency of only 0.026%. We found an 8x

decrease in the proportion of unique variants after transformation, identifying 16,307 unique variants in the final library. The most common sequence in the final library had a prevalence of 0.067%, whilst the average sequence prevalence was 0.006%. This reduction in sequence diversity was expected, as the number of bacterial cells during transformation was much smaller than the number of possible distinct plasmids. For an anticipated c/c_{gel} value in the order of 10, we require a maximum prevalence below 10% to allow for gelation[18] and to suppress polymerization[21]. In the final plasmid library, the maximum sequence prevalence (0.067%) is more than two orders of magnitude lower than required. Thus, each plasmid has a negligible chance of randomly encountering a complementary lock & key domain on a different plasmid in solution.

To further confirm the high selectivity of individual variants for their complements on the same plasmid backbone, we conducted thermodynamic predictions on the top 1000 most abundant sequences in the final library (Figure 3d, Supplementary Data 2). The calculated Gibbs free energies (ΔG) demonstrated that the variants have high affinity towards their reverse complements, with an average $MFE_{selective}$ of -113 ± 10 kJ mol^{-1} (cf. diagonal entries in Figure 3d), in excellent agreement with the initial estimate for a randomized lock & key sequence. In contrast, the non-complementary pairs averaged a $MFE_{non\text{-}selective}$ of -26 ± 6 kJ mol^{-1} (cf. off-diagonal entries in Figure 3d). This large difference (ΔMFE ~ 87 kJ mol^{-1}) confirms that the intramolecular pairing of lock & key domains is highly selective and the final DLK plasmid library exhibits near-ideal orthogonal binding under thermodynamic equilibrium conditions.

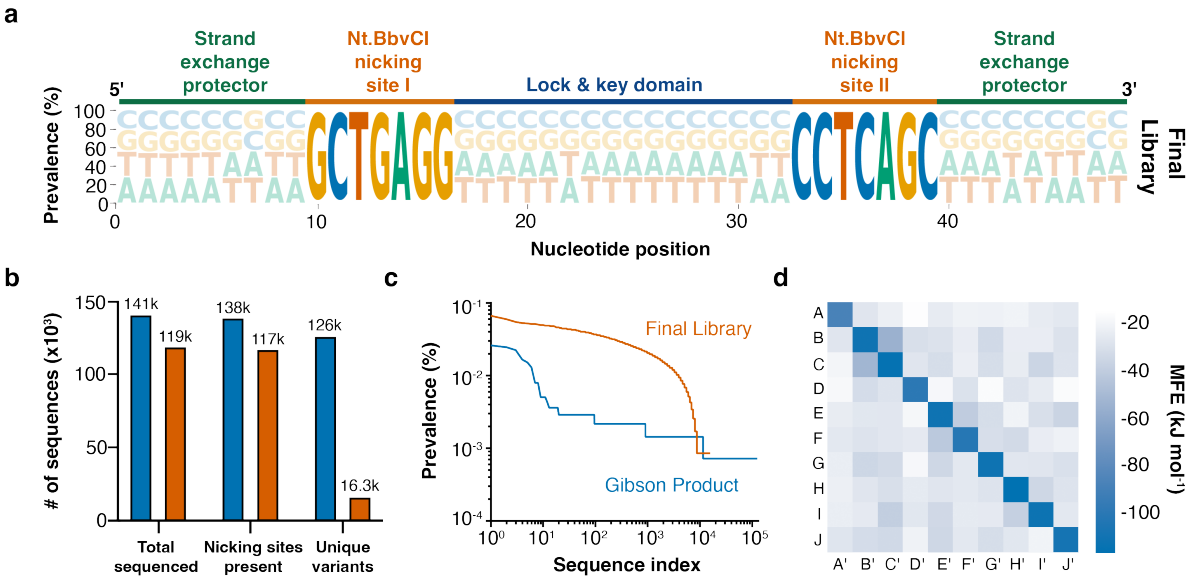

Figure 3. Next-generation sequencing reveals high sequence diversity and binding orthogonality of the *DLK* insert. a) Sequence logo for the comparison of the prevalence of the four canonical bases within the *DLK* insert in the final library after transformation. The size of each letter corresponds to the probability of the indicated nucleotide to appear at that position. **b)** Next-generation sequencing data for a single batch of plasmid products. The total number of sequences were merged from paired end reads on the Illumina MiSeq platform. Blue bars indicate the sequences from the Gibson product, and orange bars indicate the sequences from the final library. **c)** Comparison of the prevalence between sequence variants (with nicking sites present) of the Gibson product and the final library, in descending order. **d)** Heatmap showing the predicted MFE for a small subset of *DLK* variants along the diagonal and their reverse complements at equilibrium. A larger matrix showing all 10^6 predicted hybridization interactions between the 1000 most abundant DLK sequences is shown in Supplementary Data 2.

AFM and cryo-SEM show DNA plasmids and their network structure

To better understand the structural characteristics of the plasmids, we performed atomic force microscopy (AFM) imaging of *PVS10-DLK* plasmids before and after nicking. The plasmids were deposited onto a mica surface from a dilute solution well below the predicted overlap concentration. For non-nicked *PVS10-DLK*, we observed intact, typically supercoiled, circular strands with an average height of approximately 2 nm, matching to the characteristic thickness of a DNA duplex (Figure 4a, c). After nicking with *Nt.BbvCI*, AFM imaging shows similar 2-nm thick DNA fibers (Figure 4b, c). Unlike the original plasmids, some nicked plasmids were observed to have free terminal ends, indicating opening of the ring (Figure 4b), potentially due to shear forces opening up the activated lock & key domain during pipetting. These results further confirm that the plasmid library consists of DNA that undergoes the anticipated structural change after enzymatic nicking.

We next aimed to characterize the microscopic structure of the nicked plasmids at high concentration where the formation of an Olympic gel was anticipated. Imaging 3D molecular networks in aqueous media is challenging, since ordinary sample preparation often causes prominent material artifacts, such as network collapse due to drying or ice crystal formation due to freezing. We therefore characterized the sample by cryogenic scanning electron microscopy (cryo-SEM), a technique that reduces preparative artifacts by transforming and maintaining the specimen in a vitrified state[41]. To this end, a nicked plasmid sample was concentrated to 0.25 wt%—approximately twice the predicted c_{gel} value—and concatenated by thermal annealing. The annealed product was subsequently frozen at high pressure to maintain the hydrated state and to conserve fine structural features within the gel (cf. Methods section).

During imaging, the sample was subjected to sublimation of water at -90°C to reveal more of the material's internal structure[42]. The images show a mesh-like, interconnected network that is akin to network structures observed in conventional hydrogels[9,41] (Figure 4d). The prolonged sublimation at -90°C caused local deformations that created pores within the gel network. This effect exposed fine strands of material that can be seen to occasionally span across gaps in the gel (Figure 4d, insets 1 and 2), which we attribute to plasmids or plasmid bundles that are stretched out as the vitrified water slowly retracts during sublimation. The observed interconnected structure with interstitial cavities supports the notion that the plasmid strands form mechanically stable connections within the gel network.

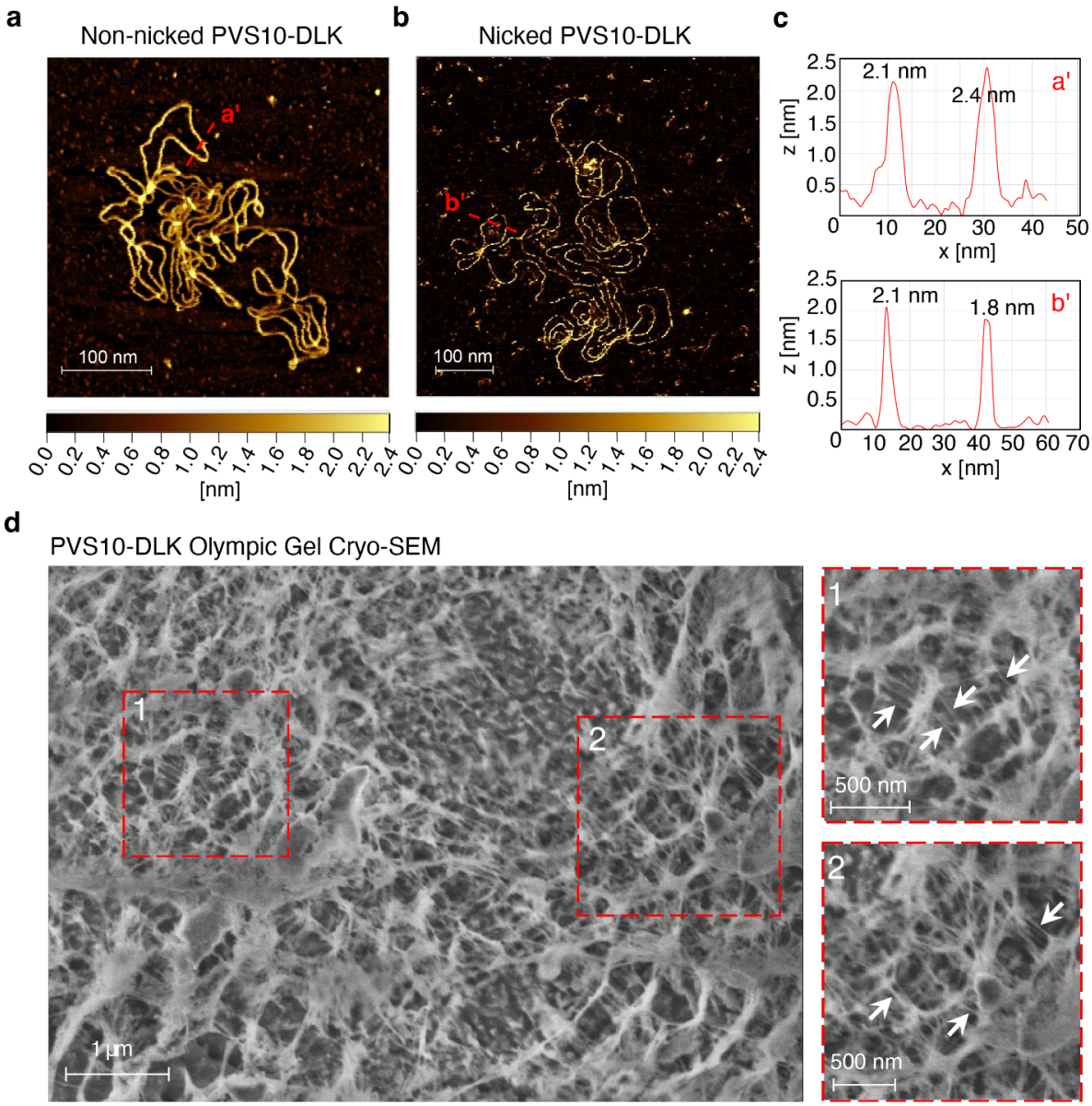

Figure 4. Microscopic characterization reveals the structure of plasmid rings and their interconnected molecular network. a) AFM images of single *PVS10-DLK* plasmids before and **b)** after nicking. **c)** Line profiles extracted from the dashed lines in (a) and (b) indicating the height of the plasmids. **d)** Cryo-SEM image of the surface of 0.25 wt% *PVS10-DLK* after annealing into an Olympic gel. Arrows indicate suspected plasmids or plasmid bundles that are stretched out due to mechanical deformation of the network in response to sublimation.

Computer simulations predict trends in mechanical and physical properties

To understand the mechanical properties of the concatenated networks, we carried out large-scale computer simulations in which randomly concatenated polymer rings with monodisperse size were sheared at varying applied stress, σ (Figure 5a, Section S1). For optimal performance, the simulations were carried out for flexible polymers at a high polymer concentration while varying the degree of polymerization (N). This yields in effect a variation of the overlap number P and the average number of concatenations per ring, f_n, over a similar range as in the experimentally measured samples.

In the simulations, the strain (γ) was computed for different applied stresses until an equilibrium state was reached (Figure S1, S3). The resulting stress-strain data of the strongly concatenated samples (Figure 5b) reveals a sub-linear stress-strain relation $\sigma \propto \gamma^{0.78\pm0.03}$ over a broad range of strains $\gamma \gtrsim 1$. The observed exponent falls in between the linear dependence expected for entanglement-free systems and the exponent of ½ as predicted in the tube model for entanglements in networks[43]. At large strains, deviations towards a larger effective exponent can be expected from the finite extensibility of the polymers[44]. Therefore, the data at the largest applied stress were excluded from the fit. At the lowest applied forces, we observe an increasing strain (indicating an increased "slip length") for increasing degree of polymerization of the rings. This behavior crosses over to a universal stress-strain relation at strains in the order of 100% or larger.

The increased strain for Olympic gels at low applied forces had been previously predicted[13], however, questions remain regarding the cross-over towards larger applied stress. A larger slip length with increasing *N* agrees qualitatively with the predictions of the slip link model for rubber elasticity[45,46]. It is difficult to extract such a dependence from stress-strain data of conventional networks due to the additional contribution from the cross-links. We anticipate that our deformation data contributes valuable information on the deformation behavior of entangled networks and may help to improve existing models for rubber elasticity[43]. Moreover, the present set of simulation data clarifies that rheological data at low strains for the samples with a large number of concatenations deserve particular attention. Finally, we simulated the deformation of the less concatenated samples with N = 128 and N = 64. For N = 128 (Figure S2), a clearly lower modulus with a linear stress-strain relation was observed (see discussion in section S1), whereas equilibrium strain was not reached for the N = 64 sample within the available simulation time.

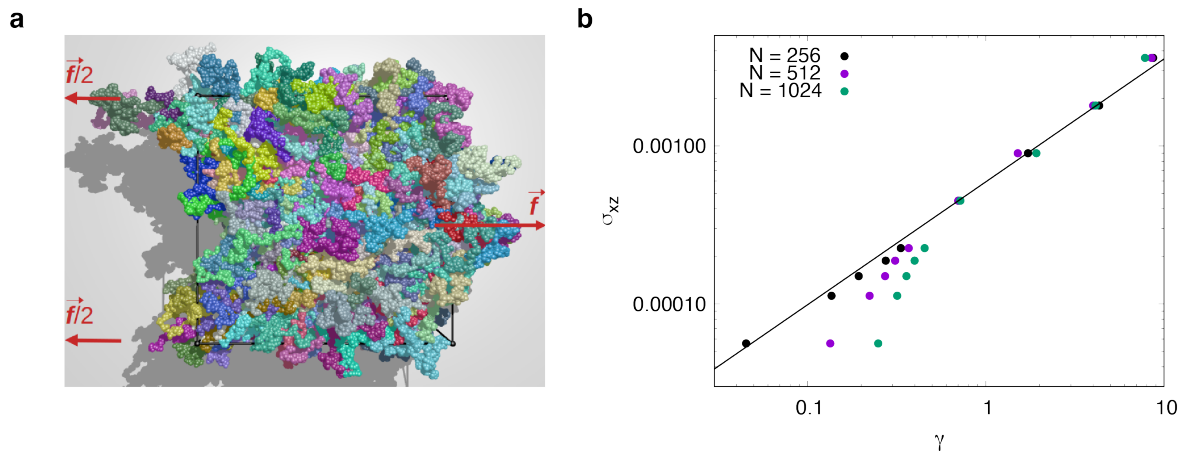

Figure 5. Computer simulations predict physical properties of the Olympic gel under different mechanical strains and varying degrees of concatenations. a) Example for a sheared Olympic gel with N = 1024, f = 0.0036 k_BT per unit length, and an average shear of 0.72. The applied force pulls the middle of the sample to the right and the top and bottom to the left. Each ring carries a random color. Rings are displayed with respect to the center of mass position at the beginning of the shear considering periodic boundary conditions. **b)** Simulation results of ideal concatenated rings under shear stress σ_{xz} (in k_BT per unit volume) for N = 256, 521, 1024, referring to different degrees of concatenation. The line indicates $\sigma \propto \gamma^{0.78}$.

The Olympic gel exhibits unique swelling characteristics

To characterize the macroscopic material characteristics of the *PVS10-DLK* library experimentally, we first compared the swelling and dissolution properties of nicked and non-nicked plasmid samples. The samples were stained with a DNA-binding dye, exposed to an excess of solvent, and subsequently imaged in a confocal microscope (Figure 6a, b and Supplementary Sections S5 and S6). All non-nicked plasmid samples dispersed within 48 hours, even at the highest concentration (0.8 wt%), demonstrating that the rings neither crosslink nor entangle permanently (Supplementary Video 2). The time scale of the dispersion is in good agreement with the predicted diffusion time scale for free plasmid DNA strands (Section S5). In contrast, the nicked samples exhibited a strongly concentration-dependent behavior: at high concentrations with $c > c_{gel}$ they swell to an equilibrium and do not further expand or disperse (Supplementary Video 1). Samples below this concentration threshold disperse over time, similar to the non-nicked plasmids. This finding demonstrates that the nicked plasmids form a permanently connected network only above the critical concentration where ring concatenation is expected.

The measured volume change during swelling further corroborates the topological nature of the material (Figure 6b and Section S6). Classical cross-linked polymer gels are predicted to swell to larger volumes when prepared at a higher polymer content[44]. In contrast, for entangled polymer networks, a constant volume change independent of preparation conditions can be anticipated (Section S6). The data in Figure 6b indicate a distinctly different behavior: the volume change is larger for the less concentrated gel (cf. 0.25 wt% and 0.8 wt% nicked samples), which neither agrees with the classically cross-linked gels nor a purely entangled network. Instead, the swelling behavior is in qualitative agreement with predictions that account for the material's unconventional network connectivity, where the number of concatenations increases (and thus the capacity for swelling decreases) with increasing plasmid concentration. A detailed discussion of this effect is provided in Supplementary Section S6.

Rheology validates the predicted trends for Olympic gel viscoelasticity

To study the mechanical properties of the gel, a set of nicked *PVS10-DLK* plasmid samples was prepared above c_{gel} (0.125 wt% – 0.8 wt%) and characterized by a broad set of rheological experiments. To promote the transient opening and closing of the rings prior to the rheology experiment, all samples were annealed at 60°C on the rheometer before measuring at 20°C (cf. Methods). Analogously prepared non-nicked plasmid samples at the same concentrations were used as a reference system. The systematic comparison between nicked and non-nicked plasmids aimed to isolate the effect of true mechanical interlocking from *transient* plasmid entanglements.

In all nicked samples, the storage modulus (G') exceeded the loss modulus (G") over a wide range of frequencies, confirming that stable and consistent gels were formed (Figure 6f). A peak in the G'' data was observed at ~0.25 Hz and ~0.1 Hz for the two highest concentrations, 0.5 wt% and 0.8 wt%, respectively. This peak corresponds to the relaxation of residual linear chains, that is, ~10% of rings that have not closed (cf. Sections S3, S4). In mixtures of cyclic and linear polymers of the same molar mass, this particular relaxation is the slowest process[47,48]. Thus, the G' data at the lowest measured frequency (1 mHz) can be considered as equilibrium data. This equilibrium G' data of the nicked samples matches the expected concentration scaling of semi-dilute entangled solutions ($G' \propto c^{2.3}$) (Figure 6c) and not the scaling for conventional gels $G' \propto c$ (cf. Section S4). A quantitative analysis based upon

the slip-tube model of rubber elasticity provides an alternate estimate for f_n, which exceeds our original estimate using computer simulation data and plasmid conformations by only 12% (see Section S4 for details). This finding confirms the consistency of our analysis, and it demonstrates that the elastic behavior of the samples is dominated by entanglements as expected for Olympic gels.

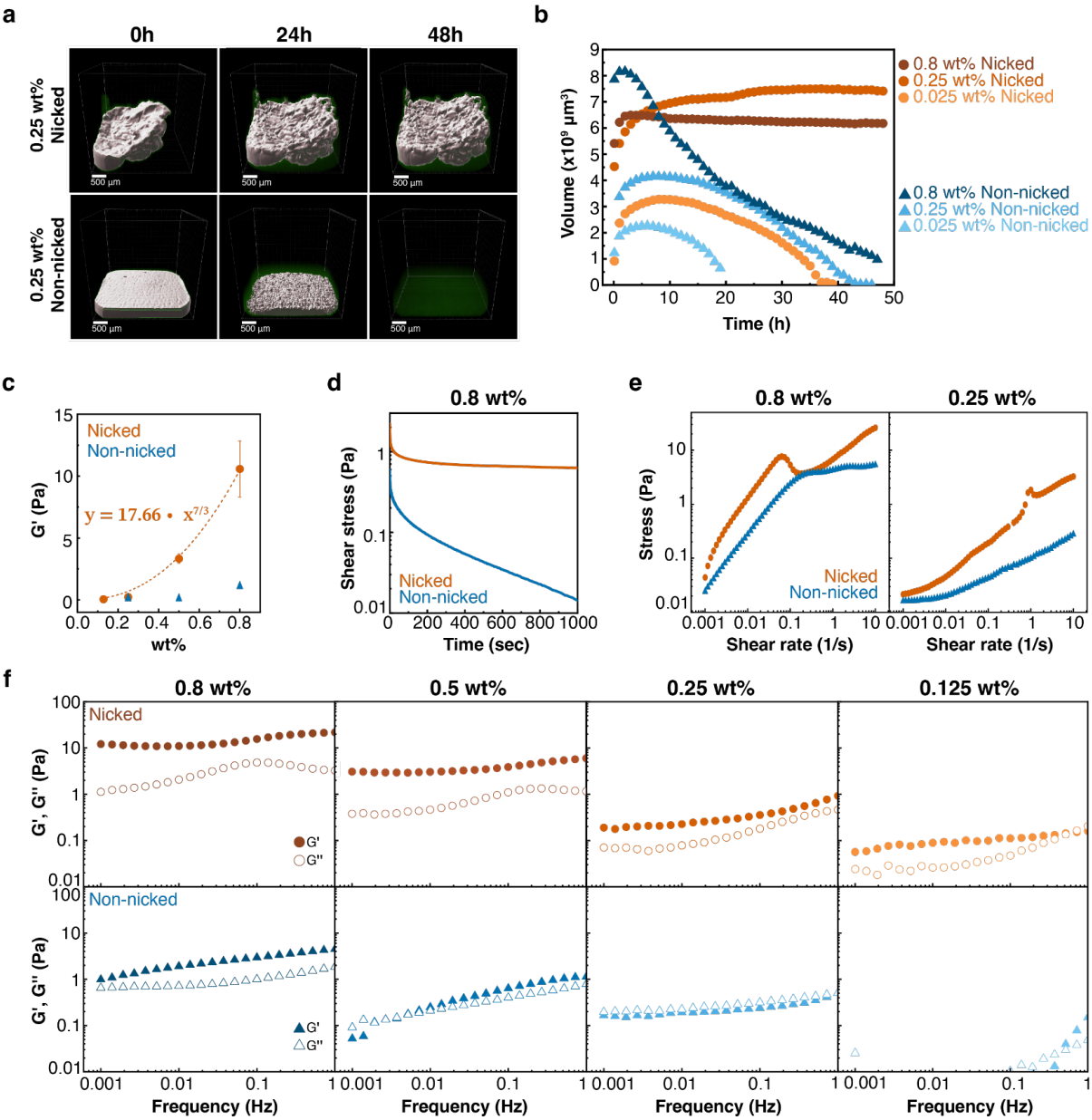

Figure 6. Rheology and confocal microscopy demonstrate the mechanical effect of plasmid concatenation and unconventional swelling characteristics of the Olympic gel. a) Confocal images of the Olympic gel swelling in buffer (top row) and dissolution of the non-nicked control plasmid solution under identical concentration and buffer conditions (bottom row). The gel volume is rendered with white surface; DNA-binding dye is shown in green. **b)** Swelling of plasmids immersed in 2xTE, 50mM NaCl for 48 hours**. c)** Plot of the storage modulus, G', of plasmids measured at 1% strain and 0.001 Hz in the frequency sweeps. Data are shown as the mean ± s.d. (n=2). The dashed line and equation correspond to the analytical expression for the entanglement model. **d)** Stress-relaxation curves of plasmids at 20°C. The shear stress was recorded over time at a fixed strain of 15%. **e)** Flow curve (stress vs. shear rate) of 0.8 wt% and 0.25 wt% plasmids. **f)** Frequency sweeps of plasmids at 1% strain at 20°C after annealing.

In contrast to the nicked plasmids, the G' curve of non-nicked plasmids dropped with decreasing frequency. In all samples except for the highest concentration (0.8 wt%), G' was lower than G'' at 1 mHz. Moreover, it was on average about one order of magnitude lower than for the nicked plasmids (Figure 6c, f). This difference highlights the dominant contribution of concatenation to the Olympic gel's elasticity. Surprisingly, the frequency data of the non-nicked plasmids at the highest concentration was more characteristic of a reversible gel than of a polymer solution, suggesting that additional weak attractive interactions between plasmids are involved. This phenomenon may be attributed to "tip bubbles", short segments of single-stranded DNA that can form in supercoiled plasmid DNA[49,50] (Figure S7). As they comprise unpaired sections of DNA, tip bubbles could weakly associate with each other. The rheology data of non-nicked samples are consistent with a reversible gel consisting of weakly binding DNA supercoils that are reinforced by entrapping relaxed cyclic DNA (cf. Section S4). The existence of a reversible gel due to tip bubbles may also account for previously unexplained experimental results for mixtures of supercoiled and cyclic DNA in the literature[51].

Nicked and non-nicked samples were further subjected to step-strain experiments to study their stress-relaxation behavior (Figure 6d). Non-nicked *PVS10-DLK* samples exhibited a simple exponential decay with a characteristic relaxation constant (τ) in the order of $\tau \approx 10$ s. The nicked *PVS10-DLK* showed a more complex relaxation profile: a similar decay to the non-nicked samples is observed for the first few seconds, but an additional long-time decay contribution is present that is characteristic for a gel converging to a non-zero storage modulus. A substantial part of the deformation energy is therefore stored elastically beyond the time scale of the experiment, as expected for the *DLK* design, in which the lock & key domains are expected to be firmly closed at room temperature.

In addition to oscillatory and step-strain experiments, we also subjected the material to rotational rheology. Flow curves show that nicked plasmids exhibit substantially higher resistance to deformation than non-nicked samples (Figure 6e). Nicked samples additionally exhibited a *yield point* with a sharply bent curve that was not present in non-nicked samples. This behavior could be explained either by wall slip or by fractures occurring within the gel due to the force opening lock & key domains mechanically[52] at large deformations. The strain amplitude at the yield point coincides with the drop of G' in the amplitude sweeps (Figure S9). Therefore, an analysis of G' at amplitudes exceeding this yield point will not provide reliable information of the Olympic gel. For the 0.8 wt% non-nicked sample, the subtle transition that occurs at high deformation could be explained by rupturing of the tip bubbles or disentanglement of the plasmids. The amplitude sweeps (Figure S9) of non-nicked plasmids show that the samples at higher concentrations are gels that either flow or might develop wall slip at strains around 100%. In contrast, the non-nicked sample at the lowest concentration is a liquid on the time scale of the experiment. Such a solid-liquid transition is expected for reversible gels somewhat above the overlap concentration[53], in agreement with the experimental data (Section S4).

Temperature-dependent rheology of the non-nicked samples shows a significant drop in G' when gradually heated (Figure S8), which is consistent with a weakening of the hypothesized tip bubble interactions. However, the data is complicated by other factors, such as temperature-dependent changes of the stiffness and branching structure of the supercoiled DNA (section S4)[54]. Nicked plasmid samples show only a slight softening of the gel when heated, suggesting that only a small fraction of lock & key domains is open at a given time at temperatures below 60°C. All nicked plasmid samples became stiffer after returning

to 20°C, suggesting that the annealing step nevertheless promoted ring opening and subsequent concatenation.

Overall, the rheological data support the formation of a stable Olympic gel from nicked *PVS10-DLK* plasmids at concentrations ≥ 0.125 wt%. Non-nicked samples are fluid at 0.25 wt% or below, but form a weak reversible gel at higher concentrations. Gelation of non-nicked samples at high concentrations is possibly caused by associations between tip-bubbles of the branched and supercoiled plasmid DNA. Further discussions and a quantitative analysis of the rheology experiments are provided in Section S4.

Conclusions

In the present paper, we have combined the tools of synthetic biology, DNA nanotechnology, computer simulations, and theoretical polymer physics to synthesize and elucidate the properties of an Olympic gel—a new form of soft matter with unique properties. The key innovation is the use of highly diversified DNA recognition sites ("lock & key domains") that were integrated into plasmid backbones and activated through enzymatic nicking. The lock & key domains serve as reactive termini that cause activated plasmids to favor self-cyclization over polymerization, even at high concentrations. In contrast to previous studies, this strategy allows efficient purification of the material and subsequent gelation while precluding the spurious formation of classical crosslinks. This approach allowed an accurate characterization and investigation into the physical properties of Olympic gels as compared to conventionally crosslinked networks.

Through microscopic imaging (AFM, cryo-SEM, and confocal microscopy) and macroscopic characterization (swelling and rheology), we have confirmed that Olympic gelation takes place if and only if the plasmid library is activated by nicking and sufficiently concentrated to allow random concatenation above the predicted ring overlap concentration. We observe a unique effect of the swelling equilibrium in which a smaller degree of swelling is observed for gels prepared at higher concentrations, opposite to the trend seen for conventional gels. We anticipate that our current experimental data and future rheological studies into this new material platform will contribute valuable information on the deformation behavior of purely entangled networks and help to improve existing models for rubber elasticity[43].

Besides its function as a model system for ideal entangled molecular networks, the creation of Olympic gels composed of genetic material directly proposes interesting potential applications for the fields of synthetic biology and bioengineering. In particular, sequences encoding for therapeutically relevant molecules, such as mRNA (e.g., for COVID or cancer vaccines), aptamers, or peptides can be included on the plasmid backbone. Owing to the free movement of the plasmid DNA, these molecules can be perpetually expressed within Olympic gel particles via rolling circle amplification, in essence creating artificial microreactors[55] that can deliver molecules at high concentration to specific target sites. Olympic gel particles could also act as artificial nuclei in synthetic cells in a similar manner as the topologically interlocked kinetoplast functions as the store of mitochondrial genes in *Kinetoplastea.*

Methods

Initial thermodynamic prediction for the lock & key domain hybridization. To estimate thermodynamic parameters of the plasmid ring closure, we carried out an initial nearest-

neighbor thermodynamic prediction for the 20 nt sticky end using the NUPACK software package (version 4.0.1.11)[34]. The prediction was based on the sequence $GGN_{16}CC$, where N_{16} was represented by a randomized sequence (ACTTAGTCACTGTGGC) along with its complement. For this pair of strands, the MFE values were calculated using the equation $MFE_{calculated} = MFE_{x,y} – MFE_x – MFE_y$, where $MFE_{x,y}$ is the predicted minimum free energy of the hybridized product, and MFE_x and MFE_y are the secondary structure energies of each of the two strands, respectively. The model parameters were set to T = 20 °C and 50 mM NaCl, with a maximum complex size set to 2. MFE was predicted as -114 kJ mol^{-1} (~46 k_BT).

***PVS10-DLK* plasmid cloning.** Cloning of the *PVS10-DLK* plasmid library was performed using a *PVS10* plasmid (AddGene 104398) and our single-stranded *DLK* insert (synthesized by Integrated DNA Technologies) as follows. The *PVS10* plasmid was digested with NcoI-HF and SbfI-HF enzymes according to manufacturer's instructions (New England Biolabs). The resulting linear fragment was purified by gel extraction from agarose gel (Qiagen). *DLK* was inserted into the digested and purified *PVS10* fragment via Gibson assembly using HiFi DNA Assembly Master Mix (New England Biolabs). *PVS10-DLK* was subsequently transformed into 5-alpha *E. coli* cells (New England Biolabs) followed by overnight growth at 37°C on Luria broth agar supplemented with 50 µg/mL ampicillin (LB-Amp). Four colonies were selected for further outgrowth overnight at 37°C in 5 mL of LB-Amp media. Plasmid DNA was extracted over a QIAprep Spin Miniprep column (Qiagen). To verify cloning efficiency, a digestion test was performed using NotI-HF and BbvCI enzymes (New England Biolabs). Digestion reactions were run on a 1% w/v agarose gel to confirm the correct digestion pattern (Figure 2b).

Olympic gel preparation. Upon successful cloning verification, we proceeded with large-scale growth of plasmid libraries. Five separate transformations of *PVS10-DLK* were inoculated into 3 mL of LB-Amp media, grown for 8 hours at 37°C, then inoculated into a total of 2.4 L of LB-Amp media. This culture was outgrown for 16-18 hours at 37°C. Cell culture was centrifuged at 4,000 rpm for 10 minutes. After removing the supernatant, plasmid DNA was extracted and purified from pellets over a ZymoPURE™ II Plasmid Gigaprep column (Zymo) and recovered in nuclease-free water. Half of the purified *PVS10-DLK* solution was nicked with *Nt.BbvCI* enzyme (New England Biolabs) over 72 hours at 37°C. To confirm successful nicking, we performed a digestion test on 500 ng of non-nicked and nicked *PVS10-DLK* with *HindIII* enzyme in NEBuffer r2.1 (New England Biolabs). Digestion products were run on a 1% w/v alkaline denaturing agarose gel to confirm the correct digestion pattern. After confirmation of the successful nicking, *Nt.BbvCI* was inactivated with addition of EDTA at a final concentration of 20 mM. Non-nicked and nicked *PVS10-DLK* samples were then dialyzed through a 50 kDa cutoff membrane filter into 1 mM Tris-HCl, 0.1 mM EDTA, and 2.5 mM NaCl at pH 8.0. Samples were then further concentrated according to the desired test concentrations (0.025 wt%, 0.05 wt%, 0.125 wt%, 0.25 wt%, 0.5 wt%, or 0.8 wt%) by reducing the volume as required by vacuum evaporation at room temperature. Buffer conditions for all samples were adjusted to 20 mM Tris-HCl, 2 mM EDTA, 50 mM NaCl, pH 8.0. To create the Olympic gel, nicked *PVS10-DLK* solutions were annealed near the estimated melting temperature of the lock & key domain (at either 55°C or 60°C) to transiently open the plasmids, followed by incubation at 20°C to anneal plasmids into an interlinked gel.

Gel-shift assay. In order to confirm proper concatenation, a gel-shift assay was performed on non-nicked and nicked *PVS10-DLK* samples at all concentrations. Samples were incubated at 50°C for 20 minutes and then incubated at 20°C overnight. Shortly before loading, annealed samples were diluted in the loading buffer (100 mM Tris-HCl, 2 mM EDTA,

and 50 mM NaCl) to required concentrations. 50 ng of each sample were loaded in a 0.5% w/v agarose gel, run at 100 V for 2-3 hours, and imaged on a Typhoon™ FLA 9500 imager.

Next-generation sequencing. The Gibson assembly product and final plasmid library isolated after Gigaprep were sequenced using NGSelect Amplicon 2nd PCR sequencing on the Illumina MiSeq with 2 x 300 bp reads. Initial PCR amplification was conducted using primers with TruSeq universal adapters for NGS specified by Eurofins Genomics. The PCR amplification was conducted in a 25 µl reaction volume using Q5® Hot Start High-Fidelity Master Mix (NEB, Cat. #M0494) using recommended primer concentrations of 0.5 µM each. The solution was initially annealed at 98 °C for 1 minute, followed by 30 cycles of 10 seconds at 98 °C, 30 seconds at 60 °C, 35 seconds at 72 °C, and a final extension at 72 °C for 2 minutes. The sequences were merged using FLASH (v 2.2.00)[56] and subsequently converted to FASTA and Tabular format using usegalaxy.org[57]. A custom python script was used to identify instances of *Nt.BbvCI* nicking sites (GCTGAGG & CCTCAGC), extract sequences of interest (Supplementary Code 1), and identify unique sequence variants and their frequencies. The base-wise variation was analyzed by generating a base-wise frequency matrix and plotted using Logomaker[58].

Thermodynamic simulations based on sequencing data. A library of 1000 sequences was generated by extracting the 500 most prevalent sequence variants from the NGS data, extracting the lock & key variants as $GGN_{16}CC$, and appending the respective reverse complements using a custom Python script. An additional library containing reverse complements of these sequences was generated. The MFE values for all explicit lock & key pairs were calculated against all possible lock & key combinations in the library with the NUPACK software package (version 4.0.1.11)[34], using the same parameters as described above.

Atomic Force Microscopy. Sample preparation protocols were adapted from Ref. [59]. Non-nicked *PVS10-DLK* double-stranded plasmid DNA was diluted in 10 mM Tris-HCL pH 8.0 (Sigma-Aldrich) buffer to 3 ng/µL. Nicked *PVS10-DLK* double-stranded plasmid DNA was diluted in the same buffer to 0.005 ng/µL. A freshly cleaved mica disc was covered with 25 µL of 20 mM $NiCl_2$ (Sigma-Aldrich), 25 µL of 10 mM Tris-HCl pH 8.0 buffer, and 7 µL of the diluted *PVS10-DLK* sample. The disc was incubated for 30 minutes at room temperature, followed by addition of 50 µL of 10 mM Tris-HCl pH 8.0 to bring the final $NiCl_2$ concentration to 5 mM. AFM imaging was performed in liquid buffer (10 mM Tris-HCl pH 8.0 and 5 mM $NiCl_2$). Peak Force Tapping imaging was performed on a Dimension FastScan AFM system (Bruker) in the ScanAsyst in Fluid - HiRes mode using ScanAsyst-Fluid+ high-resolution cantilevers (Bruker). Peak Force amplitude was set to 6 nm at a frequency of 8 kHz. The Peak Force setpoint was set to 0.005 V corresponding to 200 pN in force. High resolution images of adsorbed plasmids were taken at a scan size of 400 x 400 nm^2 or less at a scan rate of 0.994 Hz and 512 samples/line.

Cryo-Scanning Electron Microscopy. Cryo-SEM imaging was performed on a Zeiss Crossbeam 550 SEM fitted with a Quorum nitrogen gas-cooled cold stage for imaging of samples under cryogenic conditions. Olympic gel samples were prepared at 0.25 wt% in 20 mM Tris-HCl, 2 mM EDTA, and 50 mM NaCl. 2 µL of sample were subjected to high-pressure freezing[42] on a Leica EM ICE High Pressure Freezer and subsequently stored in liquid nitrogen. A Quorum PP3010T cryogenic preparation system was used to mount samples under liquid nitrogen and vacuum conditions for subsequent transfer to the cryo-preparation chamber and loading onto the pre-cooled SEM stage. Sample surfaces were imaged under vacuum without etching or coating at low acceleration voltage and probe current (1.8 kV and 25 pA

respectively) at 13.8k x magnification and working distance of 4.6 mm. Samples were sublimed by slowly warming the SEM stage, with images taken at a final temperature -90°C.

Computer simulations. Ideal Olympic gels made of mono-disperse flexible polymer rings were prepared as described in Ref. [18] using the bond fluctuation model (BFM)[60,61] in the LeMonADE implementation on graphical processing units (GPU)[62,63]. A polymer volume fraction of φ=0.5 was chosen on a cubic lattice of size 256^3. The degrees of polymerization of the cyclic polymers were N=64, 128, 256, 512, and 1024. Shear simulations were performed as described in Refs. [44,64]. Details of the simulations and the analysis are discussed in section S1 of the supplemental information.

Swelling measurements. Samples were stained with 50x SYBR Gold (Thermo Fisher) prior to the measurement. Before swelling, samples were annealed at 60°C for 30 minutes, cooled to 20°C at -3°C/min, and then incubated at 20°C overnight. Shortly before imaging, 5 µL of each sample were dispensed into a glass-bottom 384-well plate (Greiner Bio-One). Each sample was immersed in 100 µL of 20 mM Tris-HCl, 2 mM EDTA, and 50 mM NaCl. Images were acquired every hour for 48 hours at 4x magnification on the Andor Dragonfly confocal microscope. The gel volume was quantified using IMARIS software (Oxford Instruments) via the surface wizard under a uniform threshold.

Rheology. Viscoelasticity measurements were conducted using an Anton Paar MCR301 rheometer with a 25 mm diameter cone-plate geometry (cone angle 0.5°). Temperature control was ensured by installing a Peltier system PTD-200 (Anton Paar) within the measurement area. The chamber is equipped with a solvent trap and a vapor lock to prevent evaporation artifacts. A wet paper cylinder was placed around the plate's circumference to maintain high humidity inside the chamber. The annealing protocol started with holding the *PVS10-DLK* solution at equilibrium at 20°C for 5 min, followed by heating steps from 20°C to 60°C at 3°C/min, and then incubation at 60°C for 20 min. The samples were then cooled to 20°C at 3°C/min and held at 20°C for 20 min, all at 1% strain and 1 Hz. Frequency sweeps were conducted from 0.001 Hz to 100 Hz at 1% strain, while amplitude sweeps were performed from 0.1% to 1000% strain at 1 Hz. Stress-relaxation properties were measured at 15% strain, where the strain was kept constant while recording shear stress over time. Stress-strain curves were determined by shearing rotationally at increased shear rate from 0.001 s^{-1} to 10 s^{-1} as the respective shear stress was recorded.

Acknowledgements. E.K. acknowledges funding by the Federal Ministry of Education and Research of Germany (BMBF) in the program NanoMatFutur (grant no. 13XP5098). M.L. acknowledges funding by the Deutsche Forschungsgemeinschaft (DFG, grant # 329888557). J.-U.S. was supported by the DFG under Germany's Excellence Strategy (EXC2068−390729961, Cluster of Excellence Physics of Life of TU Dresden). We would like to thank Dr. Lothar Steeb for useful discussions and Pelobiotech GmbH that serve as an industry partner. The authors thank Dr. Ilka Hermes and Qiong Li for assistance with AFM measurements, Vinolia Dmello for cryo-SEM sample preparation, Dr. Luca Bertinetti and Prof. Dr. Yael Politi for assistance with cryo-SEM measurements and data analysis, and Dr. Günter Auernhammer for helpful discussions on rheology experiments. We also thank Dr. Michele Marass for giving valuable feedback on the draft. Parts of Figure 2b were created with BioRender.com.

Author contributions. E.K., J.-U.S. and M.L. conceived and designed the study. A.A. and S.S. designed, carried out, and analyzed cloning experiments and production of plasmids for the Olympic gel and control samples. S.S. performed the AFM measurements. Y.-H.P. performed

the rheological experiments, swelling measurements, and the gel-shift assay. K.G. performed the next-generation sequencing experiments and data analysis, thermodynamic calculations, and participated in the design of cloning experiments. M.S. and T.M. carried out computer simulations. C.F. performed the cryo-SEM experiments. S.S., A.A., Y.-.H.P., K.G., M.L., J.-U.S. and E.K. participated in data analysis. S.S., M.L., and E.K. wrote the manuscript with input from all authors.

Competing interests The authors declare no competing interests.

References

1. Osada, Y. & Gong, J.-P. Soft and Wet Materials: Polymer Gels. *Adv. Mater.* **10**, 827–837 (1998).
2. Sangeetha, N. M. & Maitra, U. Supramolecular gels: Functions and uses. *Chem. Soc. Rev.* **34**, 821–836 (2005).
3. Hirst, A. R., Escuder, B., Miravet, J. F. & Smith, D. K. High-Tech Applications of Self-Assembling Supramolecular Nanostructured Gel-Phase Materials: From Regenerative Medicine to Electronic Devices. *Angew. Chem. Int. Ed.* **47**, 8002–8018 (2008).
4. Qiu, Y. & Park, K. Environment-sensitive hydrogels for drug delivery. *Adv. Drug Deliv. Rev.* **53**, 321–339 (2001).
5. Kim, J. *et al.* Wearable smart sensor systems integrated on soft contact lenses for wireless ocular diagnostics. *Nat. Commun.* **8**, 14997 (2017).
6. Lee, K. Y. & Mooney, D. J. Hydrogels for Tissue Engineering. *Chem. Rev.* **101**, 1869–1880 (2001).
7. Krieg, E., Weissman, H., Shirman, E., Shimoni, E. & Rybtchinski, B. A recyclable supramolecular membrane for size-selective separation of nanoparticles. *Nat. Nanotechnol.* **6**, 141–146 (2011).
8. Beebe, D. J. *et al.* Functional hydrogel structures for autonomous flow control inside microfluidic channels. *Nature* **404**, 588–590 (2000).
9. Krieg, E. *et al.* Supramolecular Gel Based on a Perylene Diimide Dye: Multiple Stimuli Responsiveness, Robustness, and Photofunction. *J. Am. Chem. Soc.* **131**, 14365–14373 (2009).
10. Flory, P. J. *Principles of Polymer Chemistry*. (Cornell University Press, Ithaca, NY, 1953).
11. De Gennes, P. G. *Scaling Concepts in Polymer Physics*. (Cornell University Press, Ithaka and London, 1979).
12. Hart, L. F. *et al.* Material properties and applications of mechanically interlocked polymers. *Nat. Rev. Mater.* **6**, 508–530 (2021).
13. Vilgis, T. A. & Otto, M. Elasticity of entangled polymer loops: Olympic gels. *Phys. Rev. E* **56**, R1314–R1317 (1997).
14. Lang, M., Fischer, J., Werner, M. & Sommer, J.-U. Swelling of Olympic Gels. *Phys. Rev. Lett.* **112**, 238001 (2014).
15. Shapiro, T. A. & Englund, P. T. The Structure and Replication of Kinetoplast Dna. *Annu. Rev. Microbiol.* **49**, 117–143 (1995).
16. He, P., Katan, A. J., Tubiana, L., Dekker, C. & Michieletto, D. Single-Molecule Structure and Topology of Kinetoplast DNA Networks. *Phys. Rev. X* **13**, 021010 (2023).

17. Hoffmann, A. *et al.* Molecular model of the mitochondrial genome segregation machinery in Trypanosoma brucei. *Proc. Natl. Acad. Sci.* **115**, E1809–E1818 (2018).
18. Fischer, J., Lang, M. & Sommer, J.-U. The formation and structure of Olympic gels. *J. Chem. Phys.* **143**, 243114 (2015).
19. Ubertini, M. A. & Rosa, A. Computer simulations of melts of ring polymers with nonconserved topology: A dynamic Monte Carlo lattice model. *Phys. Rev. E* **104**, 054503 (2021).
20. Bonato, A., Marenduzzo, D., Michieletto, D. & Orlandini, E. Topological gelation of reconnecting polymers. *Proc. Natl. Acad. Sci.* **119**, e2207728119 (2022).
21. Lang, M. & Kumar, K. S. Simple and General Approach for Reversible Condensation Polymerization with Cyclization. *Macromolecules* **54**, 7021–7035 (2021).
22. Pickett, G. T. DNA-origami technique for olympic gels. *Europhys. Lett. EPL* **76**, 616–622 (2006).
23. Raphaifl, E., Gay, C. & De Gennes, P. G. Progressive Construction of an 'Olympic' Gel. *J. Stat. Phys.* **89**, 111–118 (1997).
24. Endo, K. & Yamanaka, T. Copolymerization of Lipoic Acid with 1,2-Dithiane and Characterization of the Copolymer as an Interlocked Cyclic Polymer. *Macromolecules* **39**, 4038–4043 (2006).
25. Endo, K., Shiroi, T., Murata, N., Kojima, G. & Yamanaka, T. Synthesis and Characterization of Poly(1,2-dithiane). *Macromolecules* **37**, 3143–3150 (2004).
26. Krajina, B. A., Zhu, A., Heilshorn, S. C. & Spakowitz, A. J. Active DNA Olympic Hydrogels Driven by Topoisomerase Activity. *Phys. Rev. Lett.* **121**, 148001 (2018).
27. Kim, Y. S. *et al.* Gelation of the genome by topoisomerase II targeting anticancer agents. *Soft Matter* **9**, 1656–1663 (2013).
28. Note: Ref. 26 demonstrates that Topoisomerase II causes a notable degree of plasmid concatenations. However, their data also shows that (1) a major fraction of plasmids likely remained non-concatenated (Suppl. Fig. S2 in ref. 26), and (2) the complex modulus (G*) drastically decreases when the material is exposed to Proteinase K, an enzyme that digests Topoisomerase II (Suppl. Fig. S3 in ref. 26). The latter observation highlights that Topoisomerase II itself forms classical crosslinks that dominate the gel's mechanical characteristics, as the authors correctly note. The authors assume that the digestion of Topoisomerase II by Proteinase K is complete and the remaining G* is therefore a result of a purely topological network. However, the completeness of the digestion was not demonstrated, and appears unlikely, since the presence of EDTA in the reaction (Suppl. Sect. I.F in ref. 26) would have a strong inhibitory effect on Proteinase K.
29. Speed, S. K., Gupta, K., Peng, Y.-H., Hsiao, S. K. & Krieg, E. Programmable polymer materials empowered by DNA nanotechnology. *J. Polym. Sci.* **61**, 1713–1729 (2023).
30. Peng, Y.-H. *et al.* Dynamic matrices with DNA-encoded viscoelasticity for cell and organoid culture. *Nat. Nanotechnol.* **18**, 1463–1473 (2023).
31. Wong, C.-H. & Zimmerman, S. C. Orthogonality in organic, polymer, and supramolecular chemistry: from Merrifield to click chemistry. *Chem. Commun.* **49**, 1679–1695 (2013).
32. Krieg, E., Bastings, M. M. C., Besenius, P. & Rybtchinski, B. Supramolecular Polymers in Aqueous Media. *Chem. Rev.* **116**, 2414–2477 (2016).
33. Xu, Q., Schlabach, M. R., Hannon, G. J. & Elledge, S. J. Design of 240,000 orthogonal 25mer DNA barcode probes. *Proc. Natl. Acad. Sci.* **106**, 2289–2294 (2009).

34. Fornace, M. E. *et al.* NUPACK: Analysis and Design of Nucleic Acid Structures, Devices, and Systems. Preprint at https://doi.org/10.26434/chemrxiv-2022-xv98l (2022).
35. Lang, M., Fischer, J. & Sommer, J.-U. Effect of Topology on the Conformations of Ring Polymers. *Macromolecules* **45**, 7642–7648 (2012).
36. Svetlov, V. & Artsimovitch, I. Purification of Bacterial RNA Polymerase: Tools and Protocols. in *Bacterial Transcriptional Control: Methods and Protocols* (eds. Artsimovitch, I. & Santangelo, T. J.) 13–29 (Springer, New York, NY, 2015). doi:10.1007/978-1-4939-2392-2_2.
37. Gibson, D. G. *et al.* Enzymatic assembly of DNA molecules up to several hundred kilobases. *Nat. Methods* **6**, 343–345 (2009).
38. Harnett, J., Weir, S. & Michieletto, D. Effects of monovalent and divalent cations on the rheology of entangled DNA. *Soft Matter* **20**, 3980–3986 (2024).
39. Levy, M. S. *et al.* Effect of shear on plasmid DNA in solution. *Bioprocess Eng.* **20**, 7–13 (1999).
40. Integrated DNA Technologies. Mixed bases | IDT. *Integrated DNA Technologies* https://eu.idtdna.com/pages/products/custom-dna-rna/mixed-bases.
41. Menger, F. M., Seredyuk, V. A., Apkarian, R. P. & Wright, E. R. Colloidal Assemblies of Branched Geminis Studied by Cryo-etch-HRSEM. *J. Am. Chem. Soc.* **124**, 12408–12409 (2002).
42. Aston, R., Sewell, K., Klein, T., Lawrie, G. & Grøndahl, L. Evaluation of the impact of freezing preparation techniques on the characterisation of alginate hydrogels by cryo-SEM. *Eur. Polym. J.* **82**, 1–15 (2016).
43. Rubinstein, M. & Panyukov, S. Elasticity of Polymer Networks. *Macromolecules* **35**, 6670–6686 (2002).
44. Rubinstein, M. & Colby, R. *Polymer Physics*. (Oxford University Press, Oxford, United Kingdom, 2004).
45. Ball, R. C., Doi, M., Edwards, S. F. & Warner, M. Elasticity of entangled networks. *Polymer* **22**, 1010–1018 (1981).
46. Edwards, S. F. & Vilgis, Th. The effect of entanglements in rubber elasticity. *Polymer* **27**, 483–492 (1986).
47. Kapnistos, M. *et al.* Unexpected power-law stress relaxation of entangled ring polymers. *Nat. Mater.* **7**, 997–1002 (2008).
48. Doi, Y. *et al.* Melt Rheology of Ring Polystyrenes with Ultrahigh Purity. *Macromolecules* **48**, 3140–3147 (2015).
49. Matek, C., Ouldridge, T. E., Doye, J. P. K. & Louis, A. A. Plectoneme tip bubbles: Coupled denaturation and writhing in supercoiled DNA. *Sci. Rep.* **5**, 7655 (2015).
50. Mitchell, J. S., Laughton, C. A. & Harris, S. A. Atomistic simulations reveal bubbles, kinks and wrinkles in supercoiled DNA. *Nucleic Acids Res.* **39**, 3928–3938 (2011).
51. Peddireddy, K. R. *et al.* Unexpected entanglement dynamics in semidilute blends of supercoiled and ring DNA. *Soft Matter* **16**, 152–161 (2020).
52. Hatch, K., Danilowicz, C., Coljee, V. & Prentiss, M. Demonstration that the shear force required to separate short double-stranded DNA does not increase significantly with sequence length for sequences longer than 25 base pairs. *Phys. Rev. E* **78**, 011920 (2008).

53. Kumar, K. S. & Lang, M. Reversible Networks Made of Star Polymers: Mean-Field Treatment with Consideration of Finite Loops. *Macromolecules* **56**, 7166–7183 (2023).
54. Marko, J. F. & Siggia, E. D. Statistical mechanics of supercoiled DNA. *Phys. Rev. E* **52**, 2912–2938 (1995).
55. Hahn, J., Chou, L. Y. T., Sørensen, R. S., Guerra, R. M. & Shih, W. M. Extrusion of RNA from a DNA-Origami-Based Nanofactory. *ACS Nano* **14**, 1550–1559 (2020).
56. Magoč, T. & Salzberg, S. L. FLASH: fast length adjustment of short reads to improve genome assemblies. *Bioinforma. Oxf. Engl.* **27**, 2957–2963 (2011).
57. The Galaxy Community. The Galaxy platform for accessible, reproducible and collaborative biomedical analyses: 2022 update. *Nucleic Acids Res.* **50**, W345–W351 (2022).
58. Tareen, A. & Kinney, J. B. Logomaker: beautiful sequence logos in Python. *Bioinformatics* **36**, 2272–2274 (2020).
59. Pyne, A., Thompson, R., Leung, C., Roy, D. & Hoogenboom, B. W. Single-Molecule Reconstruction of Oligonucleotide Secondary Structure by Atomic Force Microscopy. *Small* **10**, 3257–3261 (2014).
60. Carmesin, I. & Kremer, K. The bond fluctuation method: a new effective algorithm for the dynamics of polymers in all spatial dimensions. *Macromolecules* **21**, 2819–2823 (1988).
61. Deutsch, H. P. & Binder, K. Interdiffusion and self-diffusion in polymer mixtures: A Monte Carlo study. *J. Chem. Phys.* **94**, 2294–2304 (1991).
62. Müller, T., Wengenmayr, M., Dockhorn, R. & Knespel, M. LeMonADE-project/LeMonADE-GPU: Release v1.2. Zenodo https://doi.org/10.5281/zenodo.5513487 (2021).
63. Müller, T. *et al.* LeMonADE-project/LeMonADE: LeMonADE v2.2.2. Zenodo https://doi.org/10.5281/zenodo.5061542 (2021).
64. Lang, M. & Müller, T. On the Reference Size of Chains in a Network and the Shear Modulus of Unentangled Networks Made of Real Chains. *Macromolecules* **55**, 8950–8959 (2022).